PAPER • **OPEN ACCESS**

Upscaling from single- to multi-filament dielectric barrier discharges in pulsed operation

To cite this article: H Höft *et al* 2022 *J. Phys. D: Appl. Phys.* **55** 424003

OPEN ACCESS
IOP Publishing
Journal of Physics D: Applied Physics
J. Phys. D: Appl. Phys. **55** (2022) 424003 (13pp)
https://doi.org/10.1088/1361-6463/ac868b

Upscaling from single- to multi-filament dielectric barrier discharges in pulsed operation

H Höft[1,*], M M Becker[1], M Kettlitz[1] and R Brandenburg[1,2]

[1] Leibniz Institute for Plasma Science and Technology (INP), Felix-Hausdorff-Str. 2, Greifswald, 17489, Germany
[2] Institute of Physics, University of Rostock, Albert-Einstein-Straße 23-24, 18059 Rostock, Germany

E-mail: hans.hoeft@inp-greifswald.de

Received 7 June 2022, revised 26 July 2022
Accepted for publication 3 August 2022
Published 19 August 2022

Abstract

A study on the scalability of discharge characteristics of a single-filament dielectric barrier discharge (DBD) to a spatially one-dimensional multi-filament arrangement driven by the same high-voltage (HV) pulses was performed for a gas mixture of 0.1 vol% O_2 in N_2 at 1 bar. Both arrangements feature a 1 mm gap with dielectric-covered electrodes featuring two hemispherical alumina caps for the single-filament and two parallel alumina-tubes for the multi-filament arrangement. The DBDs were characterised by electrical measurements (for peak current, energy, and power) accompanied by iCCD and streak imaging to determine the filament number and the discharge development in the gas gap and on the surfaces. It was found that the electrical quantities scale with a constant factor between the single- and multi-filament arrangement, which is expected to be related to the filament number. In the multi-filament arrangement, the pulsed operation leads to filament formation in the entire gap in lateral direction within less than 2 ns. Furthermore, particular breakdown or discharge inception regimes were identified for the multi-filament DBDs. These regimes could be generated at the falling slope of asymmetrical HV pulses featuring e.g. a double-streamer propagation, which was previously reported for single-filament DBDs. Consequently, it was proven that the discharge manipulation by varying the HV pulse widths obtained for single-filament DBDs can also be applied in a one-dimensional multi-filament arrangement, i.e. an upscaling based on the knowledge for single-filament DBDs seems to be generally possible.

Keywords: dielectric barrier discharges, electrical and optical diagnostics, upscaling, single filament, multi filament

(Some figures may appear in colour only in the online journal)

* Author to whom any correspondence should be addressed.

1. Introduction

Dielectric barrier discharges (DBDs) are a common tool to generate non-thermal atmospheric pressure plasmas [1–3], which are used for e.g. chemical processing or gas purification [4–7]. In molecular gas mixtures, DBDs are in most cases filamentary, i.e. individual constricted discharge channels are formed, which are transient on the ns time scale [8, 9]. It was shown in various studies that the generation of reactive species is more efficient for pulsed-operated discharges than for classical sine-driven operation [10–13]. In plate-to-plate arrangements, DBDs feature a wide variety of lateral, self-organising structures and patterns, which depend e.g. on the gas mixture, the pressure and the electrode area [14, 15] Previous investigations on pulsed-driven DBDs in a single-filament arrangement have demonstrated that the breakdown and the discharge development can be directly controlled by the HV pulse width [16, 17]. By using asymmetrical HV pulses, the discharge at the subsequent HV slope is generated in a high space charge environment generated by the residual charges from the afterglow of the discharge event occurring at the previous HV slope. This residual space charge density in the gap (pre-ionisation) leads to different electric field configurations in the volume prior to the subsequent discharge inception, which is the so-called volume memory effect [18]. The pre-ionisation level can be used to determine the breakdown characteristics [19] in addition to the surface memory effect [20]. Generally, plasma-chemical reactions are mainly triggered by the physical processes within single filaments [9], while many filaments occur in DBD arrangements, which are used in practice [21]. Since it was already demonstrated that it is possible to significantly influence the plasma parameters in single-filament arrangements [19], this could be a way to initiate more selective and effective plasma-chemical processes in multi-filament arrangements. However, it is up to now unknown if the results obtained for single-filament DBDs can be directly transferred to multi-filament arrangements. In addition, open questions do not only concern the electrical breakdown in the gap, but also the interaction of volume and surface processes in multi-filament arrangements [22–26] and large scale plasma reactors [4, 5, 27]. Therefore, the central aim of this work is to clarify if the dominant effect of volume pre-ionisation for single-filament arrangements occurs also in multi-filament arrangements. For this purpose, a systematic study on the scalability of single filament characteristics to multi-filament arrangements was performed in a N_2–O_2 gas mixture at atmospheric pressure. To exclude as many side effects as possible, the same alumina was used as the dielectric barrier, while the same HV pulse source and gas mixture of 0.1 vol% O_2 in N_2 were utilised, which was used for most of the previous studies on single-filament DBDs [16, 19, 28–32]. The gas composition was chosen since the single-filament DBD is temporally very stable (low discharge inception jitter <1 ns) and especially reproducible [33] at this specific O_2/N_2 ratio due to a minimum recombination rate of positive molecular oxygen and nitrogen ions for 0.1 vol% O_2 admixture [34]. Additionally, this particular gas mixture enhances the effect of pre-ionisation, which is beneficial for a comparison of its effect on the DBD characteristics.

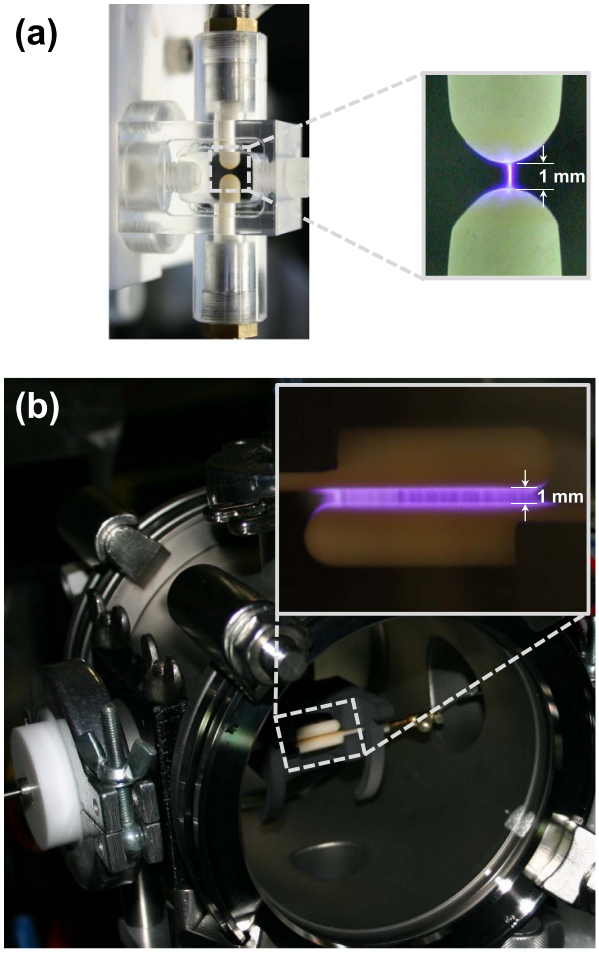

Figure 1. Plexiglas cell with the single-filament arrangement (a), stainless steel discharge chamber containing the multi-filament arrangement (b); photographs of the running DBDs in the 1 mm gap are shown for both arrangements in the respective enlargement.

The DBD will be characterised by electrical and optical diagnostics to track the discharge development in the volume and on the dielectric surfaces. The comparison of both single- and multi-filament operation will allow statements concerning the existence of comprehensive mechanisms—e.g. the pre-ionisation—to control the breakdown and the dynamics of pulsed DBDs. Additionally, a comparison of essential quantities, such as discharge current and consumed electrical energy for single- and multi-filament DBDs, will reveal if the electrical characteristics scale with the number of filaments.

2. Experimental set-up

For the purpose of directly comparing single- and multi-filament DBDs, two different arrangements were used. The single-filament DBD was ignited in a Plexiglas cell with quartz windows, which is shown in figure 1(a) and has been described in detail in [16]. It holds two hemispherical alumina-covered electrodes with 2 mm radius featuring

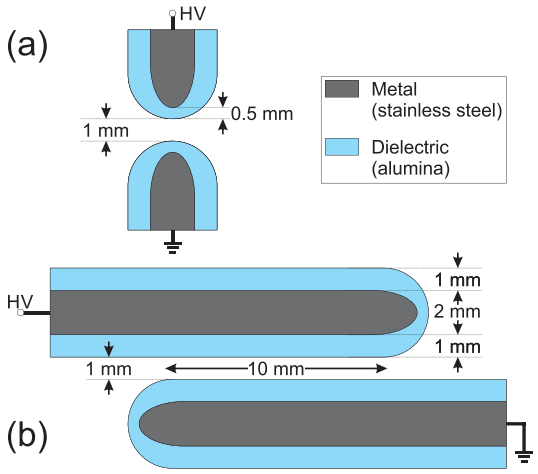

Figure 2. Schematic representation of the (a) single- and (b) multi-filament DBD arrangement, true to scale.

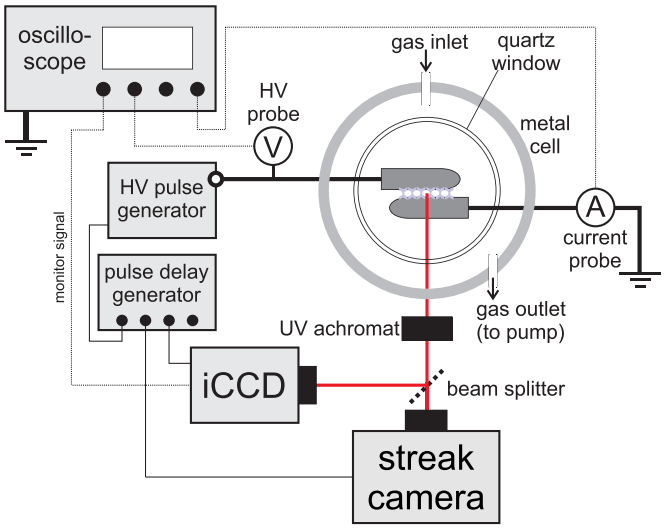

Figure 3. Sketch of the experimental set-up including diagnostics for the multi-filament arrangement, the same diagnostics were applied to the single-filament arrangement, too (only replacing the UV achromat by a long-distance microscope).

a 1 mm gas gap and 0.5 mm dielectric thickness at the tips (determined by x-ray measurements of the electrodes, schematic representation shown in figure 2(a)). This configuration geometrically forces a spatially-fixed filament position in the gap centre, see figure 1(a). The multi-filament arrangement was positioned in a pumpable stainless steel chamber with a quartz window at the front (see figure 1(b), gas inlet on the top and gas outlet at the bottom). To exclude any impact of the dielectric material on the comparison between the single- and the multi-filament DBDs, the same alumina tubes (manufacturer Friatec) were used for both arrangements. The multi-filament arrangement with 1 mm gas gap consists of two parallel alumina cylinders (4 mm outer and 2 mm inner diameter with metal rods of 2 mm diameter inside, i.e. the thickness of the dielectric in the gap d_b is 1 mm on each electrode, see figure 2(b)). Since the use of the same dielectric material was essential for the experiments, the d_b for the multi-filament arrangement is twice of that for the single-filament arrangement. Unfortunately, this could not be avoided, because there are no tubes with a wall thickness of 0.5 mm of this specific alumina commercially available (but the different d_b was taken into account in the analysis). The lateral length of the 1 mm gas gap is about 10 mm with an increasing gas gap distance at the left and right end due to the hemispherically-shaped tips (see figure 2(b)). The geometry of this arrangement is similar to the one used in [35] for the purpose of robust current peak detection.

The total gas flow through the cell was set to 100 sccm for the single-filament arrangement and to 300 sccm for the multi-filament arrangement (to compensate the bigger discharge chamber volume) by mass flow controllers connected to gas cylinders (N_2, O_2, purity 5.0 and 4.8, respectively). The O_2 concentration of 0.1 vol% in N_2 was controlled by an oxygen sensor (ZIROX SGM 7.4) for both arrangements during the experiments.

Unipolar square wave pulses with 10 kV amplitude and 10 kHz repetition frequency generated by a HV pulse source (DEI PVX-4110, 50 ns rise/fall time (10%–90%) of HV slope) were used to operate the DBDs in both arrangements. The HV pulse width t_{pulse} was varied from 0.2 to 50 μs. A fast iCCD camera (Andor iStar DH734-18U-A3) and a streak camera system (Hamamatsu C5680-21C) connected to a long-distance microscope (Questar QM100 with Quartz optics) recorded the DBD structure and the spatio-temporal development through a quartz glass window (see figure 3). The spatial resolution of both cameras was approximately 2 μm for the single filament arrangement and approximately 20 μm for the multi-filament arrangement to allow the visualisation of the complete discharge gap (using a B. Halle Nachfl. OUV 1.4.40 UV achromat instead of the QM100). The maximal temporal resolutions of the iCCD and streak camera systems were 2 ns and 20 ps, respectively. Electrical measurements were performed with fast voltage and current probes (Tektronix P6015A, and custom-build 50 Ω resistor [36]), and recorded by a digital sampling oscilloscope (Tektronix DPO 7254C, 2.5 GHz, 40 GS s^{-1}). The same electrical diagnostics were used for both arrangements.

3. Experimental results and discussion

3.1. Electrical characterisation

The applied HV waveforms with varying pulse widths are displayed over a complete period of 100 μs in figure 4(a). The pulse width ranges from 50 μs corresponding to a symmetrical HV waveform (i.e. the same time between the rising slope (RS) and subsequent falling slope (FS)) to strong asymmetrical pulses down to $t_{pulse} = 0.2$ μs, see figure 4(b). There is an individual discharge event at the RS and the subsequent falling HV slope of the unipolar pulse. They are induced by the electric field strength in the gap, which is strongly influenced by surface charges from the previous discharge, even though the polarity of the applied HV is not changing (unipolar operation) [28]. The total discharge current I_{tot} is the sum

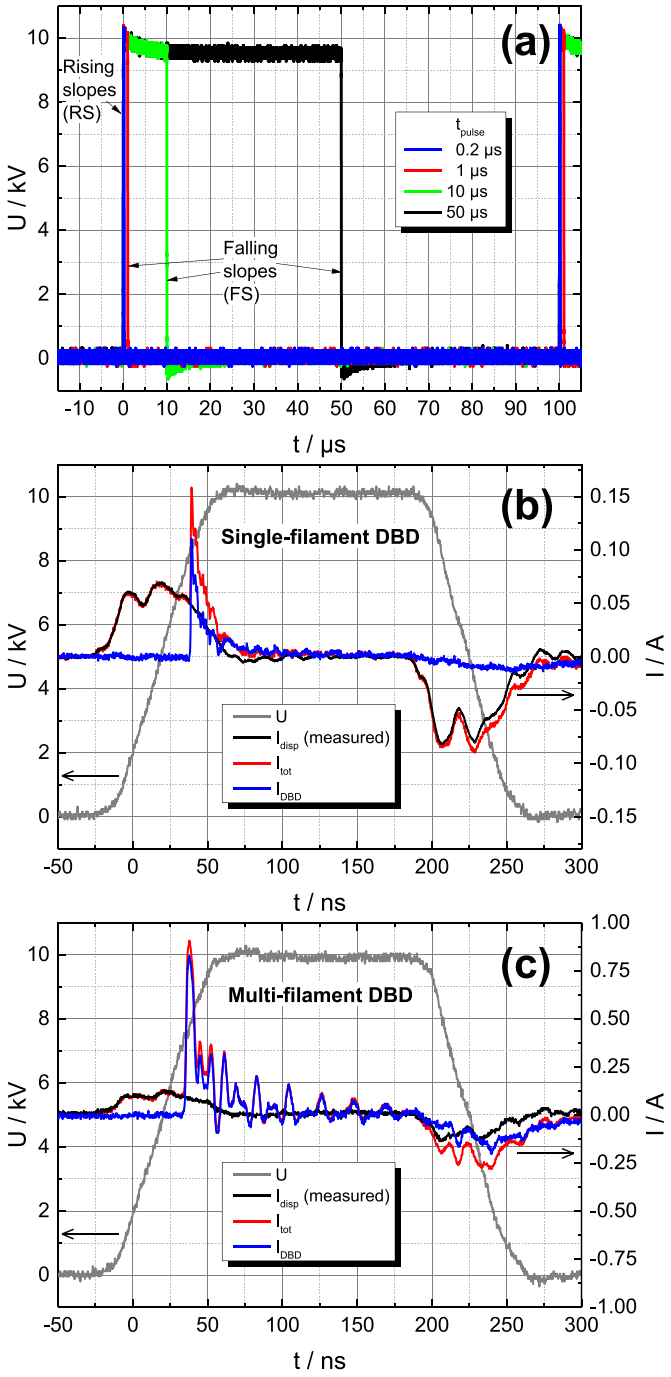

Figure 4. Overview of applied HV pulses (a) under t_{pulse} variation, and an example for a single- and multi-filament DBD with different current components (displacement (I_{disp}), total (I_{tot}) and discharge (I_{DBD}) current) at both slopes for $t_{pulse} = 0.2\ \mu s$ (b) and (c).

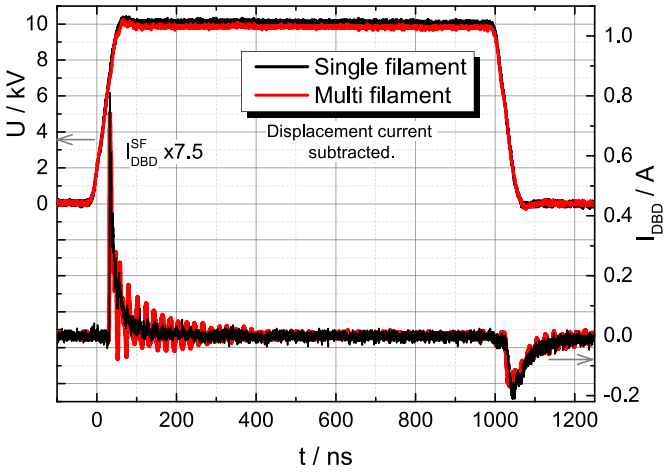

Figure 5. Voltage and current characteristics of the applied 1 μs HV pulse and the corresponding discharge current at both slopes for single- and multi-filament arrangement.

of the displacement current I_{disp} and the discharge current I_{DBD}. These components of the total current can be identified in figure 4(b) and (c) for the shortest HV pulse width. The displacement current (black curve in figures 4(b) and (c)) could be directly measured, since the discharge did not always ignite immediately after applying the HV pulse. It is obvious that the maximum value of I_{DBD} with respect to the amplitude of I_{disp} is much higher for the multi-filament arrangement compared to the single-filament arrangement. The reason for this is the fact that the discharge current peak for the multi-filament case is the superposition of multiple individual DBD channels. Although there are many channels in this multi-filament arrangement, the discharge inception jitter is about 1.5 ns at the RS, while it is below 1 ns for the single-filament DBD (both values were obtained analysing about 11 000 individual discharge events as described in [37]). This will be analysed further for the multi-filament case with respect to the discharge inception in the gap using the optical diagnostics (in section 3.4).

The oscillations on the current signals visible in figures 4(b) and (c) were induced by distortions of the steep I_{DBD} rise at the RS. Since they depend on the I_{DBD} amplitude, they are more pronounced for the multi-filament case (see figure 4(c)), but these oscillations are slightly visible for the single-filament, too (see figure 4(b)). Furthermore, it is evident that the discharge current peak at the FS of the 0.2 μs HV pulse is strongly smoothed and much lower compared to the one at the RS both for the single- and multi-filament arrangement. This is the first indication that the volume pre-ionisation plays a dominant role in both arrangements and can be directly used to control the discharge characteristics at the FS via t_{pulse} variation [19]. The excellent scalability of I_{DBD} between the single- and the multi-filament DBD is demonstrated in figure 5 for $t_{pulse} = 1\ \mu s$. Despite the different arrangement geometry the shape of the discharge current at both slopes is the same for both arrangements, i.e. the I_{DBD} of a single-filament DBD scaled by a factor of 7.5 closely resembles the discharge current for the multi-filament DBD (see figure 5). The comparison of I_{DBD} at the RS shown in figure 6 reveals a smoother rise of the current for the multi-filament case, which is due to the fact that the multiple discharge channels do not ignite simultaneously (but within few ns, see page 9). In addition, it is visible in figure 6 that the oscillations after the peak feature the same shape, which is another indication that they are most likely connected to induced distortions of the current measurement system.

In figure 7, the absolute peak values of the discharge current at the RS and FS are displayed as a function of t_{pulse} for

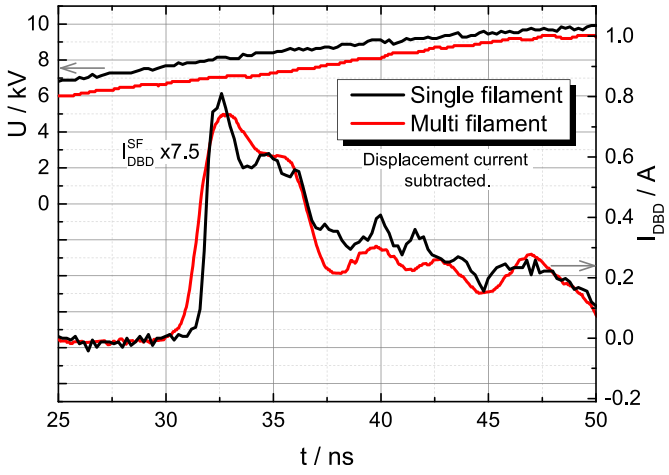

Figure 6. Comparison of the discharge current rise at the rising slope of the 1 μs HV pulse for single- and multi-filament arrangement, single-filament I_{DBD} scaled; current waveforms shifted to lay on top of each other for better comparison (both currents are synchronised with the applied voltage).

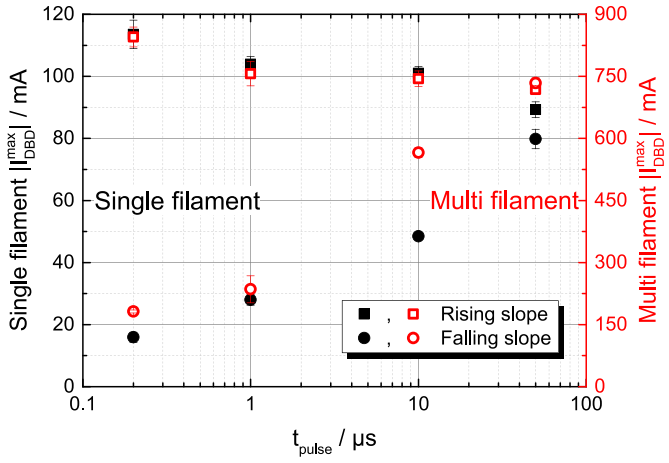

Figure 7. Distribution of maximal discharge current at rising and falling slopes for single- and multi-filament DBDs in dependence on the HV pulse width (obtained from 3077 single shots per data point); scaling factor between single- and multi-filament arrangement ≈7.5.

single- and multi-filament DBDs. The reduced impact of the pre-ionisation on the current maxima/minima with longer HV pulse width is evident for both arrangements (and approximately the same values were obtained at both slopes for a symmetrical HV pulse, i.e. $t_{pulse} = 50\,\mu$s), while a constant scaling factor of about 7.5 fits relatively well for almost all cases. The deviation at the FS for $t_{pulse} = 10\,\mu$s is an indication that for this specific case, the impact of the pre-ionisation is weaker, which can also be seen in spatial discharge emission structure (see iCCD image for $t_{pulse} = 10\,\mu$s in section 3.3 on page 7).

For the determination of the consumed electrical energy per period E_{el}, Q-U plots were used both for single- and multi-filament DBDs with different HV pulse widths, see figures 8(a) and (b). The transferred charge Q was calculated by integrating the total current over one period. The enclosed area of a Q-U plot is the equivalent of E_{el} [1]. In figure 8(c) the values of this

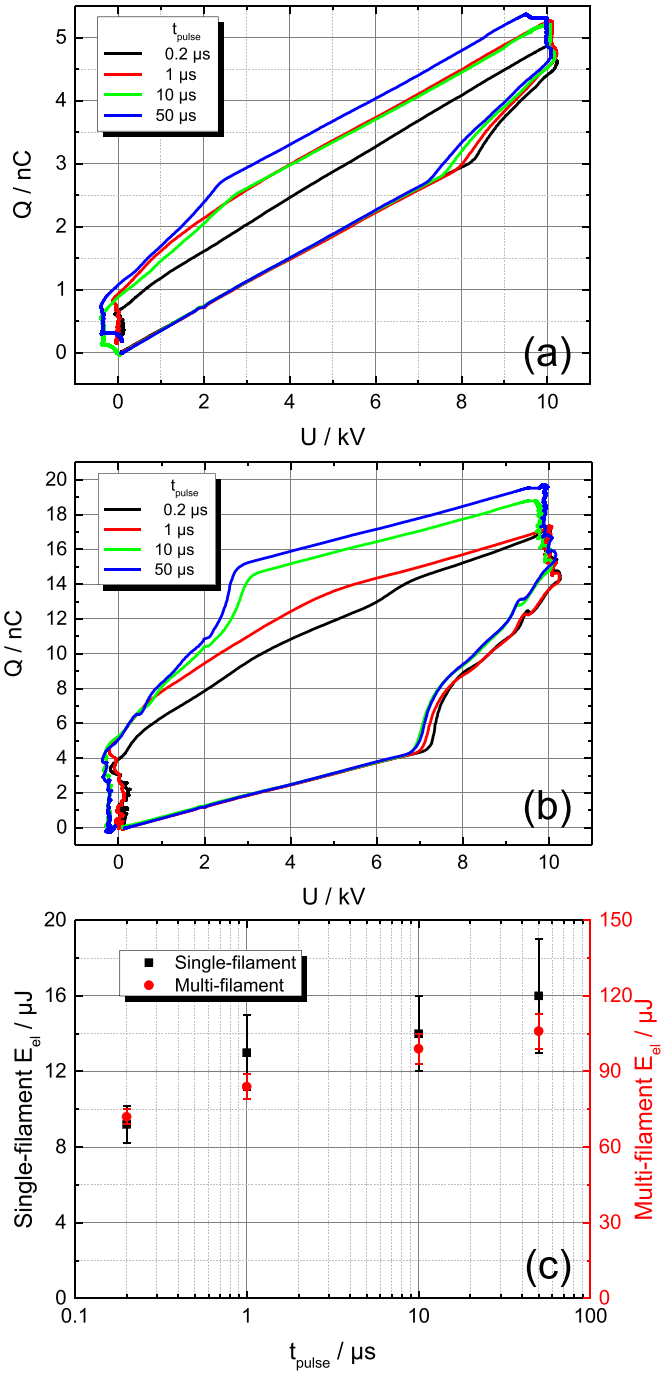

Figure 8. Q-U plots for single-filament (a) and multi-filament arrangement (b) using voltage and (integrated) current waveforms (averaged over 1000 discharge events per curve) and the calculated consumed electrical energy (c), energy scales with a factor of ≈7.5.

energy are displayed for both cases over t_{pulse}. The consumed electrical energies decrease both for single- and multi-filament DBDs with shortening of the HV pulse width. This was reported already for the single-filament case, and could be explained by the weaker discharge event at the FS due to pre-ionisation [19]. Since the same behaviour was also found for the multi-filament cases, it can therefore be also related to increasing pre-ionisation at the FS. In addition, the average electrical discharge power P_{el} can be obtained by multiplying E_{el} with the

repetition frequency. P_{el} is ranging from about 90 to 160 mW for the single-filament and from 0.7 to 1.1 W for the multi-filament DBDs. The values of E_{el} and consequently also for P_{el} for the single-filament DBDs scale with the same factor as the discharge current (approximately 7.5) and describe the dependence of E_{el} (and P_{el}) on t_{pulse} for the multi-filament DBDs quite well. When assuming that the number of filaments in the multi-filament arrangement N_{MF} is the scaling factor, the different thicknesses of the dielectric d_b have to be considered (see figure 2), i.e. the following relation reported in [38] has to be taken into account (ε_r … dielectric constant):

$$\frac{Q}{d_{gap}} \sim \frac{\varepsilon_r}{d_b}. \tag{1}$$

While the gap width d_{gap} and ε_r are the same for both arrangements, d_b is 1 mm for one electrode in the multi-filament case, but only 0.5 mm for one electrode in the single-filament case, i.e. the transferred charge in the multi-filament arrangement Q_{MF} scales with a factor of 1/2 in addition to N_{MF}:

$$Q_{MF} = \frac{1}{2} N_{MF} Q_{SF} \approx 7.5\, Q_{SF}, \tag{2}$$

with $N_{MF} = 15 \pm 2$ for all cases at the RS. This number was obtained from iCCD single shots.

Concerning the assumed scaling factor $N_{MF}/2$, it has to be noted that I_{DBD} (and consequently Q) has to be scaled with another factor depending on the capacitances of the gap and the dielectric barriers [39]. However, due to the different geometries of the discharge arrangement it is not clear if the approach of the equivalent circuit, which leads to this factor, can be directly applied here.

Nevertheless, the fact that the electrical quantities for the multi-filament DBDs can be reproduced by the quantities obtained for the single-filament DBDs by using only a constant factor, is a strong indication that the characteristics of a single-filament DBD can be directly transferred to a multi-filament arrangement, especially with respect to the impact of different pre-ionisation. It has to be noted that this constant scaling factor does not generally imply that the impact of d_b on the discharge properties is linear. In the next section, the spatio-temporal discharge development of DBDs will be analysed to evaluate if breakdown characteristics of the single-filament DBDs can be found in the multi-filament arrangement, too.

3.2. *Evaluation of the time-integrated spatial discharge structure*

In figure 9, the spectrally-integrated discharge emission structures of an individual discharge event as well as accumulated over 1000 discharges are shown for both HV slopes of the single-filament DBD. Under the investigated pulsed operation, the discharge is always filamentary, i.e. it features a thin constricted channel in the volume and spreading surface discharge channels on the dielectrics, which can be distinguished in the images of individual discharge events only. While the channel in the volume is spatially fixed (as can be seen in the accumulated images compared to the single shots), the emission on the

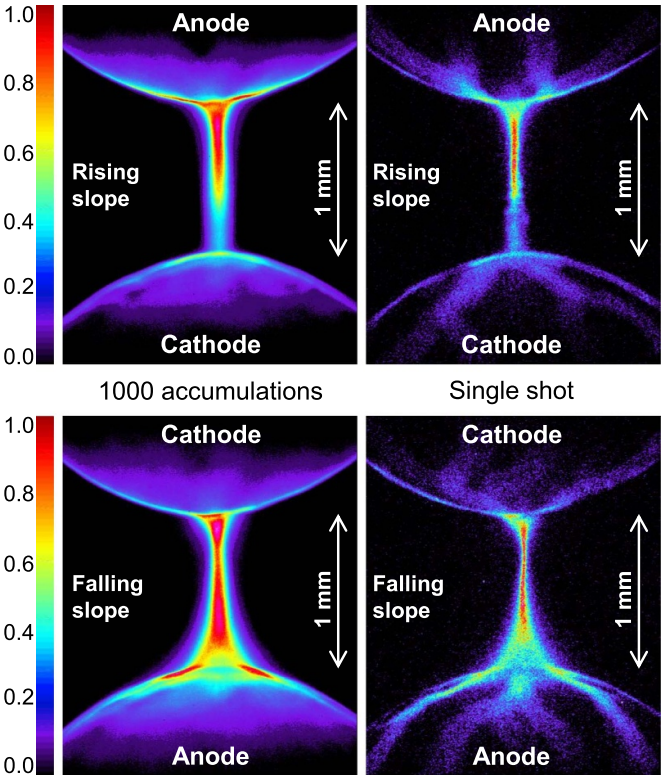

Figure 9. Overall discharge structure at both HV slopes in the single-filament arrangement for 1 μs HV pulse width and 250 ns iCCD gate; left column 1000 accumulations (with no MCP (microchannel plate) gain), right column single shot (with 200 MCP gain).

dielectric surfaces features no distinct structures; except for the footpoints, where the volume channel touches the dielectrics. This indicates that the positions of the surface discharges are changing for each individual discharge event, but they are uniformly distributed leading to the impression of an homogenous emission on the surfaces, which decays with the distance to the gas gap.

Since the iCCD images in figure 9 show the discharge emission for the case of a 1 μs HV pulse, the discharges at the FS are strongly influenced by the pre-ionisation in the gas gap caused by the preceding discharge at the RS. This leads to a special breakdown regime at the FS, which differs significantly from the regular discharge inception by a cathode-directed ionisation front (positive streamer [1, 40]), which is present at the RS [16]. The breakdown regime at the FS, which features both a cathode- and anode-directed streamer-like propagation, was already thoroughly investigated for pulsed-driven single-filament DBDs, see e.g. [17–19], and is therefore not shown here.

In the multi-filament arrangement, however, the discharge emission structure recorded by iCCD imaging is different. For all HV pulse widths at the RS, the discharges in the gap feature only indistinct constricted channels accompanied by diffuse emission within the lateral dimension of the gap, especially visible in the single-shots in figures 10(c), (g), (k) and (o). Furthermore, in the iCCD images accumulated over 1000 subsequent discharge events for the RS in figures 10(a), (e), (i) and

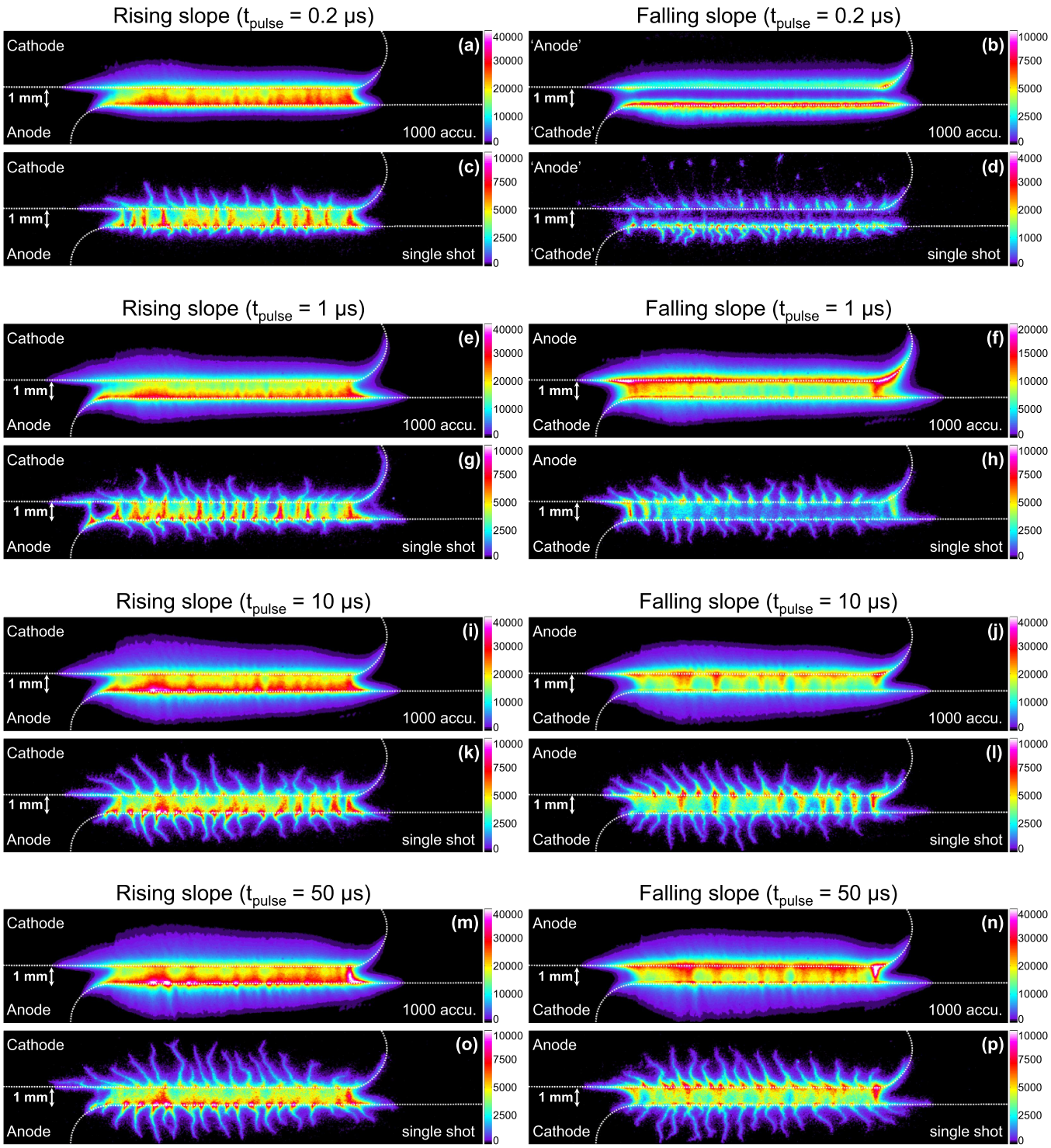

Figure 10. Overview of overall discharge structure at both HV slopes in the multi-filament arrangement for all used HV pulse widths showing accumulation of 1000 subsequent discharge events (no iCCD gain) and a single shot (iCCD gain 200), intensity scaled linearly in pseudocolour (note the different absolute intensity values), iCCD gate width 250 ns for (a)–(d) and 500 ns for (e)–(p).

(m), it can be seen that the major part of the emission is located near the anode, while a few distinct channels are visible, too. In the single-shots for the RS, it is also evident that surface discharge channels are propagating on the dielectric surface of both the anode and the cathode. Due to the fact that the images were taken side-on, the actual length of these channels on the surface is much longer than it appears in the images. This is because the electrodes are cylindrical, i.e. the surface discharges are propagating on the curvature towards the line of sight. The discharges at the FS feature different emission structures depending on the HV pulse widths. For the cases of 0.2 and 1 μs HV pulse widths, the discharges at the FS slope

ignite in high pre-ionisation in the gap generated by the previous discharge at the RS. Consequently, there is even more suppression of distinct volume discharge channels. Especially at the FS of a 0.2 μs HV pulse, the emission is dominated by the re-ignition of surface discharges on the cathode (anode at the RS), while there is only minor emission in the volume. Additionally, there seems to be some kind of 're-illumination' of the surface discharge channels tips of the previous discharge event at the RS (see the emission spots on the top of the anode surface in figure 10(d)). This is most likely caused by the electric field reconfiguration during the FS, which happens while the surface discharge channels are still conductive. This is in accordance with the observations for the single-filament DBD in [17, 19], where a similar re-ignition behaviour was reported. Since the reversal of the electric field in the gap by surface discharges is obviously not completed for the 0.2 μs case, the labels 'cathode' and 'anode' were set in quotation marks in figures 10(b) and (d). The absence of distinct volume discharge channels is also partly visible for the 1 μs HV pulse width (especially in the lateral gap centre, see figure 10(h)), while the major emission occurs here on the anode surface, not on the cathode like for the FS at the 0.2 μs case. This is an indication that the reversal of the electric field caused by deposited surface charges during the discharge at the RS is at least partly completed when the FS occurs. The discharges at the FS for 10 and 50 μs HV pulse widths feature no distinct differences compared to the ones at the RS except for the exchange of anode and cathode, i.e. they appear to be vertically mirrored. This is an indication of a reduced pre-ionisation impact for the 10 μs HV pulse width compared to the single-filament DBD, which could already be assumed from the electrical characteristics (see figures 7 and 8(c)). Generally, the impact of volume pre-ionisation is stronger in the single-filament arrangement compared to the multi-filament one, since the filament position is fixed in the gap centre, i.e. there is almost no radial movement of the discharge channel.

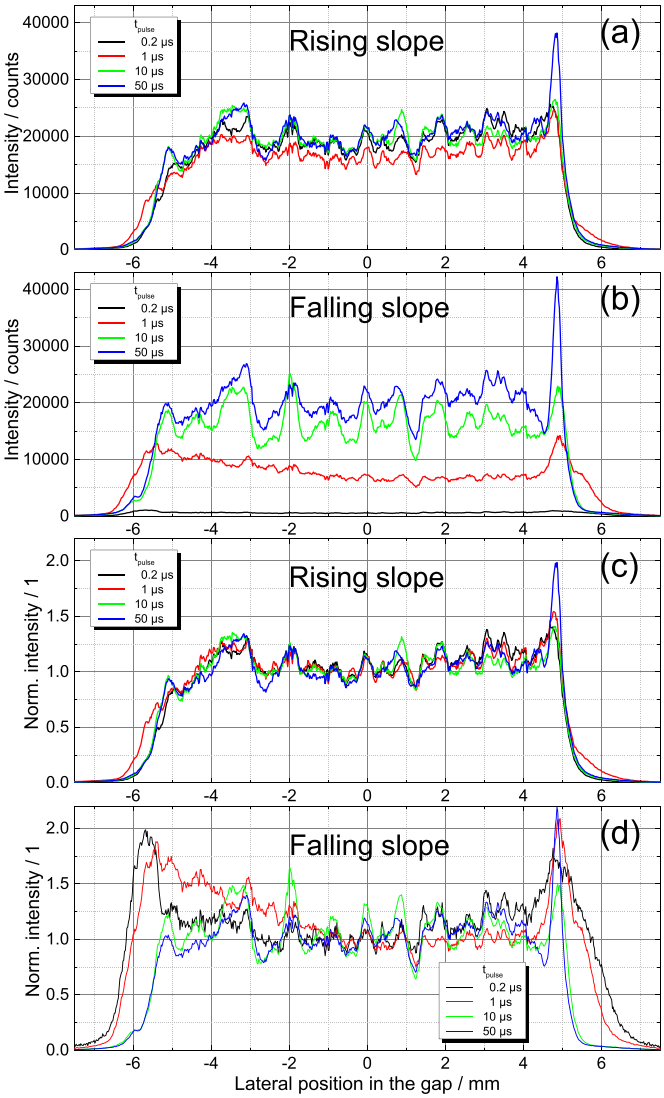

Figure 11. Lateral profiles of discharge emission in the axial centre of the gas gap (axially averaged over 80 μm) obtained from the accumulated iCCD images in figure 10, (a) and (b) show the directly comparable intensity while the intensity is normalised with respect to the mean value of the plateau in the gap centre in (c) and (d).

3.3. Analysis of the lateral emission structure for the multi-filament arrangement

The iCCD images of the discharge emission can be used to analyse the lateral position of the filament occurrence. Although there is some diffuse emission throughout the complete gap, as can be seen e.g. in figures 10(c), (g), (k), (l), (o) and (p), there seem to be some underlying lateral structures, which cannot be directly distinguished from these images. Therefore, the accumulated images were used to detect lateral structures appearing for discharges for all HV pulse widths at both HV slopes, since the accumulated iCCD recordings contain the information of the mean lateral discharge occurrence. For this purpose, a lateral profile averaged over 80 μm in the centre of the gap was extracted from all accumulated iCCD images displayed in figure 10. In figure 11, these profiles are displayed over the lateral orientation of the gap, where '0' indicates the lateral gap centre. The emission intensities displayed in figures 11(a) and (b) for the RS and FS at different HV pulse widths can be directly compared. At the RS, these intensities are approximately the same (in accordance with the similar values of the discharge current maxima, see figure 7). In addition, the peaks in these structures, indicating the mean lateral discharge channel positions, are in fair agreement. This means that, although the emission profiles are somehow blurred by the underlying diffuse emission and the spatial jitter of individual volume discharge channel positions, there are some distinct lateral positions, where the volume channels occur independent of the HV pulse width. The same is true for the FS (see figure 11(b)), i.e. the same mean lateral emission structure occurs. However, this is hardly distinguishable, since the emission intensity is significantly reduced at the FS for short HV pulse widths due to the strong impact of the pre-ionisation (which also occurs for single-filament DBDs, see [19]). For a proper comparison of the lateral discharge emission structures, the extracted emission profiles

were normalised with respect to the mean emission intensity in the gap centre in figures 11(c) and (d). While there is no big difference between the actual and normalised structures at the RS (compare figures 11(a) and (c)), the lateral profiles at the FS can be much better compared using the normalised visualisation, see figure 11(d). Although there seems to be no significant emission in the volume for the discharges at the FS for HV pulse widths of 0.2 and 1 μs (see figures 10(d) and (h)), there is a very similar underlying lateral structure. This leads to the conclusion that the mean position of the (albeit weak) volume emission occurs at the same position both at RS and FS independent of the HV pulse width. For the cases of 0.2 and 1 μs HV pulse widths, a distinct extension of the emission at the left and right end of the lateral gap was found. It corresponds to the outer regions, where the curvature of the electrodes enlarges the gap distances (see figure 2(b)). This is most likely a consequence of the increased pre-ionisation, which leads to the expansion of the discharge occurrence at the edges (however, one has to keep in mind that the intensity is much lower compared to the discharge events at the RS).

To track two discharge events at the RS and subsequent FS of the same HV pulse, streak camera measurements were performed. The axial gap centre was imaged over a lateral length of about 11 mm on the entrance slit of the streak camera to track the discharge channel positions during an individual rising and subsequent FS of the HV pulse. The streak image shows the position of discharge channels in the gap centre, i.e. it does not show the spatio-temporal development along the channel, but only the centre part of it (axially averaged over 190 μm). In figure 12(a), the result is shown exemplarily for the RS and FS of a 1 μs HV pulse in 2 μs time window. The lateral profile temporally-averaged over 30 ns at each HV slope (figure 12(b)) clearly indicates that the structure features exactly the same lateral characteristics. The intensity, however, is much lower at the FS (like in the lateral profiles obtained from the iCCD images, see figures 11(a) and (b)). This occurs for all investigated HV pulse widths, i.e. on the μs time scale, the lateral filament position is fixed at the RS and subsequent FS. Most likely, this is caused by the volume memory effect, i.e. the residual space charge density in the gap [20], since this also occurs for the short HV pulse widths, where the surface memory effect is not fully established yet.

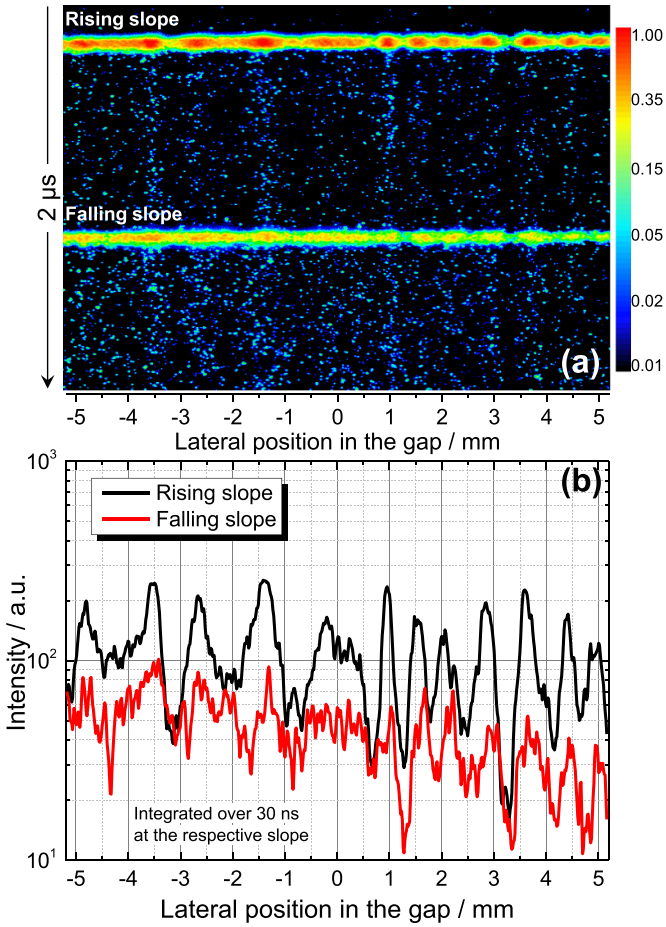

Figure 12. Filament position at the gap centre in the multi-filament arrangement for the case of a 1 μs HV pulse width (a) streak image in 2 μs window showing rising and subsequent falling slope for a single shot (log. scaled intensity in pseudo colour), (b) temporally-integrated axial profile (over 30 ns) at both slopes.

3.4. Temporal characterisation of DBDs in the multi-filament arrangement

Finally, the streak camera recordings of the discharge emission in the gap centre were used to evaluate the appearance of the discharge channels with sub-ns temporal resolution. In figure 13(a), a single-shot in a 10 ns time window is shown, where the temporal development of the central part of distinct individual discharge channels in the gap centre can clearly be distinguished. However, although the averaged streak image is blurred compared to the single-shot, the underlying lateral discharge structure discussed in the previous section is again clearly visible in figure 12(b). Note, that this streak recording was accumulated over 10^5 subsequent individual discharge events (while the profiles shown in figure 11 feature only 1000 individual discharge events). The major emission duration in the gap centre is about 3 ns (full width at half maximum) per channel, which is in accordance with measurements for a single-filament DBD [19]. This demonstrates that the discharge emission is mainly determined by the O_2 admixture to N_2 [37]. Additionally, it can be concluded from the accumulated streak image that on average, the discharge channels appear in the gap centre within less than 2 ns starting from the right side, see figure 13(b). This leads to a mean lateral 'expansion velocity' of $(5.1 \pm 0.3)\,\mathrm{mm\,ns^{-1}}$, which is in the range of the streamer propagation velocity in a single-filament arrangement (actually about two times faster). A similar lateral expansion was found in a modelling study for a DBD with a 1 mm gap [41], where the initial discharge was generated in the gap centre and expanded after the formation of the initial discharge channel. The streak camera results shown in figure 13 indicate that the lateral discharge inception in the gap occurs with only a minor delay when the breakdown voltage in the gap is reached by the fast rising applied HV. The starting point, however, is not centred, which could be a consequence

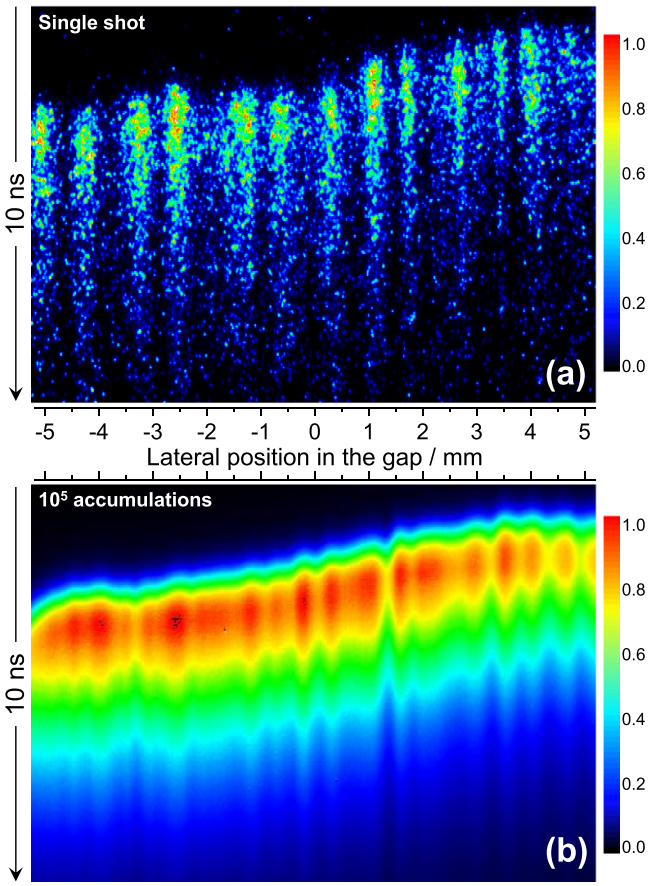

Figure 13. Lateral temporal occurrence of discharge channels in the gap centre of the multi-filament arrangement (axially averaged over 190 μm in the gap centre) at the rising slope for the case of a 1 μs HV pulse width in a 10 ns window: (a) single shot, (b) accumulation of 10^5 discharges (intensity scaled linearly in pseudo colour).

of a slightly shorter gap[1] at the lateral position around 4 mm (figure 13(b)).

Finally, the temporal discharge development in axial (vertical) direction at both the RS and FS of the HV pulse was evaluated for the different HV pulse widths under consideration. This was done using temporally-resolved iCCD images with 2 ns iCCD gate width, which were accumulated over 1000 individual discharge events at each temporal step and shifted 50 times by 1 ns resulting in a 'streak-like' image showing 50 ns of the axial discharge development displayed in figure 14. Each time step corresponds to a lateral slice averaged over 60 μm at the lateral centre of the gap (corresponding to the position '0' in figures 11–13). Although the temporal resolution is far below the one needed for a proper tracking of the streamer propagation, this visualisation of the spatio-temporal discharge development can nevertheless be used to identify different breakdown regimes, which are already well-known from single-filament DBDs [19]. For all investigated HV pulse widths, the temporal discharge characteristics at the RS feature only minor differences, i.e. a fast propagating cathode-directed streamer followed by a transient glow-like discharge in the gap with an emission maximum near the anode (as for 'classical' DBDs [40, 42]). This is in excellent agreement with the findings for the single-filament DBD [16, 19], and corresponds well to the temporal emission profiles of the streak images in the gap centre (figure 13). From this observation, it can be concluded that discharges at the RS are barely affected by the minor variations in the pre-ionisation levels as was found for single-filament DBDs [19].

At the FS, however, significant differences in the spatio-temporal discharge development are visible. For the shortest HV pulse width of 0.2 μs, there is almost no emission in the volume (in accordance with the iCCD images in figures 10(b) and (d)). Instead, there is a re-illumination of a surface discharge near the cathode (anode at the previous RS), which features a local initial maximum and lasts tenths of ns. After approximately 20 ns, a similar emission is visible on the anode (cathode at the previous RS). This is a clear indication of the strongest possible effect of residual pre-ionisation on the subsequent discharge, which is the almost complete suppression of volume streamer propagation. As a consequence, there are no distinct discharge channels in the gap, since they are formed by the propagating cathode-directed streamer. It is known from previous investigations on single-filament DBDs that this suppression is caused by a high residual electron density ($>10^{12}$ cm^{-3}), i.e. the discharge initiation does not feature volume streamers. The current in the volume is instead carried by the residual electrons [17, 18]. Furthermore, this can be seen from the low but broadened discharge current peak at the FS of the 0.2 μs pulse (see figures 4(b) and (c)). This is due to the fact that the propagation of a regular cathode-directed streamer is connected to the typical steep current rise seen for the cases with lower pre-ionisation [43].

For a HV pulse width of 1 μs, which is in the time range for positive ions to cross a 1 mm gap under the conditions (gas mixture, pressure and electric field) considered here [17, 44], a particular breakdown structure was found at the FS (see the FS for $t_{\mathrm{pulse}} = 1$ μs in figure 14). It features a short cathode-directed streamer starting at about 0.2 mm distance to the cathode and simultaneously a propagation of a negative (anode-directed) streamer with velocities on the order of 10^5 m s^{-1} (e.g. the negative streamer needed about 8 ns for 0.8 mm axial distance). Although the spatial and temporal resolutions are not as high as for the recording of the single-filament DBDs at the same HV pulse widths, it can clearly be stated that this 'double-streamer' discharge inception is very similar to the one reported for the single-filament arrangement [17]. This specific breakdown regime was related to the residual pre-ionisation, which enables this double propagation [19]. The residual space charge carrier densities generating the electric field in the volume are not as high as for $t_{\mathrm{pulse}} = 0.2$ μs (i.e. to prevent a streamer propagation), but high enough to start both cathode- and anode-directed streamers near the cathode.

The differences between the discharge development at the RS and FS for a 10 μs HV pulse width are mainly a lower cathode-directed streamer velocity and a longer discharge emission duration at the FS compared to the RS. It is barely

[1] However, this possible difference has to be less than 20 μm (which is the spatial resolution), since in the iCCD images of the illuminated multi-filament arrangement, no difference in the gas gap distance was evident.

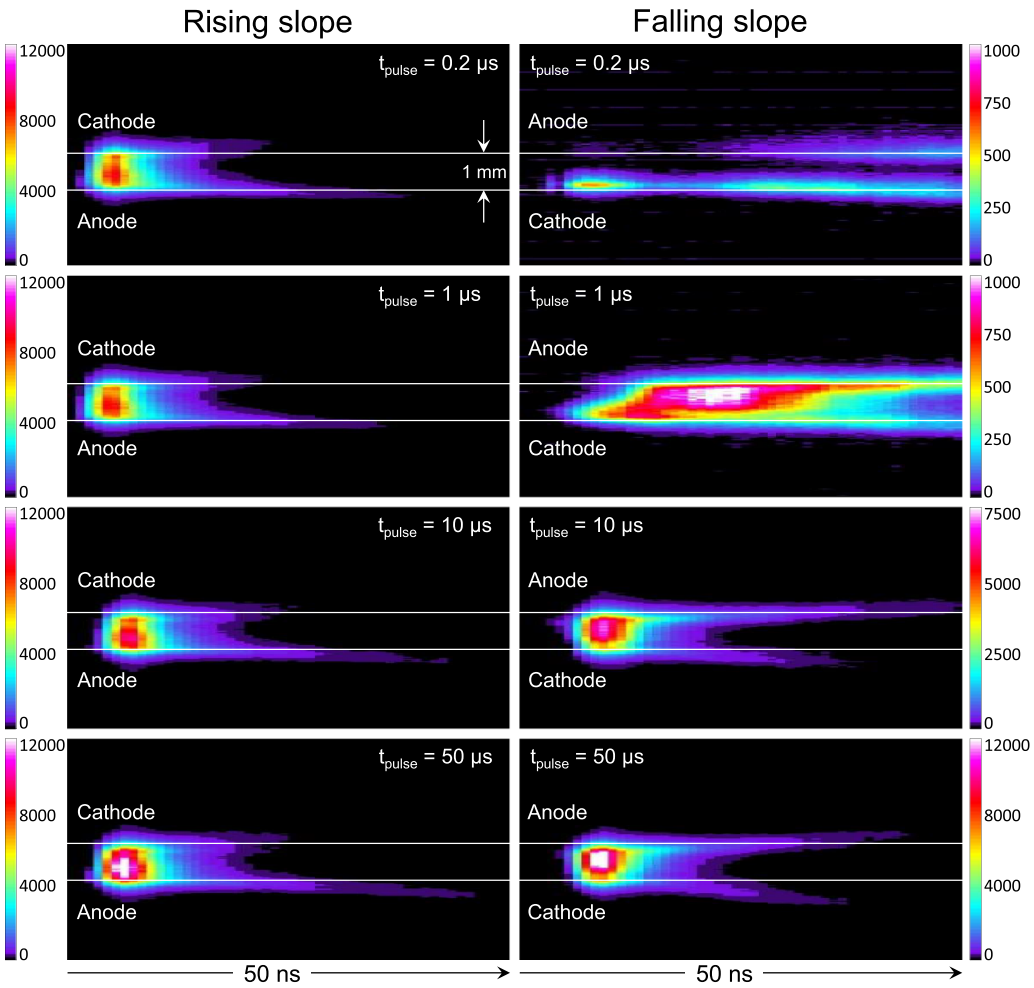

Figure 14. Spatio-temporal development in the gap centre obtained from 2 ns gate iCCD images shifted by 1 ns in the multi-filament arrangement (accumulated 1000 times per 2 ns gate), intensities linearly scaled in pseudo-colour can be directly compared.

distinguishable due to the low temporal resolution, but still visible, see figure 14, while there is no fundamental change in the breakdown regime. This is in accordance with the findings for the single-filament DBD [16], although the reduction in streamer velocity and the increase of discharge emission duration is a little weaker (which could also be seen from the comparison of the discharge current maxima, see figure 7). Most likely, this is a consequence of the not completely fixed lateral filament positions in the multi-filament arrangement. For the symmetric HV pulse width of 50 μs, however, the spatio-temporal discharge development is the same at the RS and FS (only cathode and anode are flipped vertically). This could be a consequence of the more spatially (laterally) stable filament positions for this case (see figures 11(a) and (b) for $t_{pulse} = 50\,\mu$s, compare also the intensities at both slopes).

In conclusion, these results are the final proof that a control of the discharge inception by means of HV pulse width variation can also be achieved in a multi-filament arrangement without the spatial fixation of the filament position, which enlarges the volume pre-ionisation in a single-filament arrangement.

4. Summary and outlook

In this study, a detailed comparison of pulsed-driven single- and multi-filament DBDs was performed using the same dielectric (alumina), discharge gap (1 mm), HV pulse characteristics and gas mixture (0.1 vol% O_2 in N_2). In the multi-filament arrangement, the filaments could move freely along one lateral direction, while the filament position is fixed in the single-filament arrangement. The electrical characterisation revealed that the discharge current and the consumed electrical energy E_{el} scale with a constant factor between the single- and the multi-filament DBDs, i.e. they scale with the number of filaments N_{MF} in the multi-filament case. Since the thickness of the dielectric was 1 mm for the multi-filament and 0.5 mm for the single-filament, the actual scaling factor in this study is $N_{MF}/2$. However, the constant relation for E_{el} and the discharge current development as well as its peak between single- and multi-filament DBDs is a clear indication that it is possible to directly upscale the single-filament results with respect to the number of filaments in the multi-filament arrangement. The distinct discharge control utilising

pre-ionisation by means of asymmetric HV pulses was also reproduced in the multi-filament arrangement, especially the particular 'double-streamer' mode for HV pulse widths within the range of the ion drift time ($\sim$1 μs) was found, too. Additionally, at the rising slopes of the HV pulse (i.e. low impact of pre-ionisation), the discharge channels ignite within less than 2 ns throughout the complete gap without a strong spatial jitter. This is a special feature of ns-pulsed DBDs, since the breakdown conditions are reached in the gap within a couple of ns due to the fast-rising applied HV pulse. Consequently, it was proven that most of the results obtained for single-filament DBDs can be directly transferred to multi-filament arrangements, i.e. the discharge control by varying the HV pulse width can most-likely be used also for application-relevant multi-filament reactors.

For future investigations, it is planned to study the interactions between individual filaments in pulsed-driven multi-filament DBDs, especially with respect to the surface charge dynamics. Moreover, different gas mixtures will be investigated, e.g. higher O_2 admixtures to N_2, where discharges are spatially and temporally unstable due to the reduced pre-ionisation effect induced by a high concentration of an electronegative admixture like O_2 or N_2O (i.e. a gas composition in which the recombination and collisional quenching of exciting states are more pronounced).

Data availability statement

The data that support the findings of this study will be openly available following an embargo at the following URL/DOI: https://doi.org/10.34711/inptdat.572.

Acknowledgments

This work was enabled by the DFG-funded project MultiFil (Project No. 408777255). Furthermore, the authors would like to thank M Timm and P Turski (both INP) for constructing the discharge cell holders, and J R Wubs (INP) for fruitful discussions and careful proofreading of the manuscript.

ORCID iDs

H Höft https://orcid.org/0000-0002-9224-4103
M M Becker https://orcid.org/0000-0001-9324-3236
M Kettlitz https://orcid.org/0000-0002-9216-2861
R Brandenburg https://orcid.org/0000-0003-3153-8439

References

[1] Kogelschatz U 2003 *Plasma Chem. Plasma Process.* **23** 1–46
[2] Fridman A, Chirokov A and Gutsol A 2005 *J. Phys. D: Appl. Phys.* **38** R1–R24
[3] Bruggeman P and Brandenburg R 2013 *J. Phys. D: Appl. Phys.* **46** 4001
[4] Kim H H 2004 *Plasma Process. Polym.* **1** 91–110
[5] Kogelschatz U 2007 *Plasma Process. Polym.* **4** 678–81
[6] Samukawa S *et al* 2012 *J. Phys. D: Appl. Phys.* **45** 253001
[7] Brandenburg R, Kovačević V V, Schmidt M, Basner R, Kettlitz M, Sretenović G, Obradović B, Kuraica M and Weltmann K D 2014 *Contrib. Plasma Phys.* **54** 202–14
[8] Kogelschatz U 2007 *Contrib. Plasma Phys.* **47** 80–88
[9] Brandenburg R 2017 *Plasma Sources Sci. Technol.* **26** 053001
[10] Williamson J M, Trump D D, Bletzinger P and Ganguly B N 2006 *J. Phys. D: Appl. Phys.* **39** 4400–6
[11] Panousis E, Clement F, Merbahi N, Ricard A, Yousfi M, Held B, Loiseau J F, Eichwald O and Gaboriau F 2009 *High Temp. Mater. Process.* **13** 359–72
[12] Chirumamilla V R, Hoeben W F L M, Beckers F J C M, Huiskamp T, Van Heesch E J M and Pemen A J M 2015 *Plasma Chem. Plasma Process.* **36** 487–510
[13] Laroussi M, Lu X and Keidar M 2017 *J. Appl. Phys.* **122** 020901
[14] Stollenwerk L, Amiranashvili S, Boeuf J P and Purwins H G 2007 *Eur. Phys. J.* D **44** 133–9
[15] Wild R, Schumann T and Stollenwerk L 2014 *Plasma Sources Sci. Technol.* **23** 054004
[16] Kettlitz M, Höft H, Hoder T, Reuter S, Weltmann K D and Brandenburg R 2012 *J. Phys. D: Appl. Phys.* **45** 245201
[17] Hoder T, Höft H, Kettlitz M, Weltmann K D and Brandenburg R 2012 *Phys. Plasmas* **19** 070701
[18] Nemschokmichal S *et al* 2018 *Eur. Phys. J.* D **72** 89
[19] Höft H, Kettlitz M, Becker M M, Hoder T, Loffhagen D, Brandenburg R and Weltmann K D 2014 *J. Phys. D: Appl. Phys.* **47** 465206
[20] Akishev Y, Aponin G, Balakirev A, Grushin M, Karalnik V, Petryakov A and Trushkin N 2011 *Plasma Sources Sci. Technol.* **20** 4005
[21] Kogelschatz U 2010 *J. Phys.: Conf. Ser.* **257** 012015
[22] Guikema J, Miller N, Niehof J, Klein M and Walhout M 2000 *Phys. Rev. Lett.* **85** 3817–20
[23] Stepanyan S A, Starikovskiy A Y, Popov N A and Starikovskaia S M 2014 *Plasma Sources Sci. Technol.* **23** 045003
[24] Callegari T, Bernecker B and Boeuf J P 2014 *Plasma Sources Sci. Technol.* **23** 054003
[25] van der Schans M, Sobota A and Kroesen G M W 2016 *J. Phys. D: Appl. Phys.* **49** 195204
[26] Usenov E A, Akishev Y S, Petryakov A V, Ramazanov T S, Gabdullin M T, Ashirbek A and Akil'dinova A K 2020 *Plasma Phys. Rep.* **46** 459–64
[27] Kogelschatz U 2004 *Plasma Phys. Control. Fusion* **46** 63
[28] Kettlitz M, Höft H, Hoder T, Weltmann K D and Brandenburg R 2013 *Plasma Sources Sci. Technol.* **22** 025003
[29] Höft H, Becker M M and Kettlitz M 2016 *Phys. Plasmas* **23** 033504
[30] Höft H, Becker M M, Loffhagen D and Kettlitz M 2016 *Plasma Sources Sci. Technol.* **25** 064002
[31] Höft H, Becker M M and Kettlitz M 2018 *Plasma Sources Sci. Technol.* **27** 03LT01
[32] Wubs J R, Höft H, Kettlitz M, Becker M M and Weltmann K D 2022 *Plasma Sources Sci. Technol.* **31** 035006
[33] Brandenburg R *et al* 2013 *J. Phys. D: Appl. Phys.* **46** 464015
[34] Höft H, Kettlitz M, Weltmann K D and Brandenburg R 2014 *J. Phys. D: Appl. Phys.* **47** 455202
[35] Pazderka M *et al* 2020 *J. Phys. D: Appl. Phys.* **54** 11
[36] Synek P, Zemánek M, Kudrle V and Hoder T 2018 *Plasma Sources Sci. Technol.* **27** 045008
[37] Höft H, Kettlitz M, Hoder T, Weltmann K D and Brandenburg R 2013 *J. Phys. D: Appl. Phys.* **46** 095202
[38] Gibalov V I and Pietsch G J 2000 *J. Phys. D: Appl. Phys.* **33** 2618–36

[39] Pipa A V, Koskulics J, Brandenburg R and Hoder T 2012 *Rev. Sci. Instrum.* **83** 115112
[40] Kozlov K V, Wagner H E, Brandenburg R and Michel P 2001 *J. Phys. D: Appl. Phys.* **34** 3164–76
[41] Babaeva N Y and Kushner M J 2014 *Plasma Sources Sci. Technol.* **23** 065047
[42] Gibalov V I and Pietsch G J 2012 *Plasma Sources Sci. Technol.* **21** 024010
[43] Steinle G, Neundorf D, Hiller W and Pietralla M 1999 *J. Phys. D: Appl. Phys.* **32** 1350–6
[44] Hodges R V, Varney R N and Riley J F 1985 *Phys. Rev.* A **31** 2610–20